Applied Catalysis B: Environmental 134–135 (2013) 75–82

Contents lists available at SciVerse ScienceDirect

Applied Catalysis B: Environmental

journal homepage: www.elsevier.com/locate/apcatb

Facile synthesis of MoS_3/carbon nanotube nanocomposite with high catalytic activity toward hydrogen evolution reaction

Tsung-Wu Lin[a,b,*], Chia-Jui Liu[a,b], Jeng-Yu Lin[c]

[a] Department of Chemistry, Tunghai University, No. 181, Sec. 3, Taichung Port Rd., Taichung City 40704, Taiwan
[b] Tunghai Green Energy development and management Institute (TGEI), Tunghai University, No. 181, Sec. 3, Taichung Port Rd., Taichung City 40704, Taiwan
[c] Department of Chemical Engineering, Tatung University, No. 40, Sec. 3, Chungshan North Rd., Taipei City 104, Taiwan

ARTICLE INFO

Article history:
Received 11 October 2012
Received in revised form 3 December 2012
Accepted 3 January 2013
Available online 9 January 2013

Keywords:
Molybdenum sulfide
Carbon nanotubes
Nanocomposite
Electrocatalyst
Hydrogen evolution

ABSTRACT

Hydrogen has been proposed as a future energy carrier in the transition from the current hydrocarbon economy. Exploring advanced materials for electrocatalytic and photoelectrochemical water splitting has become one of the most important issues for bulk and inexpensive hydrogen production. In this study, the nanocomposite of MoS_3 and multi-walled carbon nanotubes (MWCNTs) with the high catalytic activity toward hydrogen evolution reaction (HER) was easily synthesized using wet chemistry process. With the aid of functional groups present in MWCNTs, amorphous MoS_3 nanoparticles were highly dispersed over MWCNT surface. It was found that MoS_3 on the MWCNTs was electrochemically reduced to MoS_2 before HER and thus the amorphous MoS_2 was identified as the actual catalyst for HER. Furthermore, MoS_2 with amorphous structure exhibited the higher HER activity than crystalline MoS_2 due to the fact that the former had a higher number of exposed edges. In addition, the catalytic activity of nanocomposite of MoS_3 and MWCNTs was increased with decreasing the loading amount of MoS_3 on MWCNTs and the optimal MoS_3 loading on MWCNTs was 33 wt%. Based on the extensive transmission electron microscopy analysis and capacitance measurements, the catalytic activity of the nanocomposite was highly correlated to its active surface area which was controlled by MoS_3 morphology on MWCNT surface. The nanocomposite of MoS_3 and MWCNTs exhibited excellent HER activity with a small overpotential of $\sim$0.13 V, large cathodic currents and a Tafel slope as small as 40 mV/decade. The impedance measurements suggested that the high catalytic activity of nanocomposite of MoS_3 and MWCNTs was stemmed from the synergistic effect from the highly exposed edges of amorphous MoS_3 nanoparticles and the excellent electrical coupling to the conductive MWCNT network. Furthermore, it was found that the current density of this hybrid catalyst was decreased to 88% of the initial value after the continuous 500 cycling, which showed the reasonable stability in the long-term operation. The present work suggested that the highly active and stable nanocomposite of MoS_3 and MWCNTs showed a great potential as a low cost alternative to Pt in water splitting.

1. Introduction

The demand for environmentally friendly energy resources gradually becomes urgent and important due to climate change and the limited availability of fossil fuels. In the recent years, hydrogen has been viewed as the clean and efficient fuel source that can be used in the vehicles and fuel cells [1,2]. Although steam reforming process ($CH_4 + H_2O \rightarrow CO + 3H_2$ and $CO + H_2O \rightarrow CO_2 + H_2$) is a conventional method to produce bulk hydrogen, it has several disadvantages including the use of non-renewable energy source, the release of carbon dioxide and high reaction temperature. As a result, a lot of efforts have been devoted to producing hydrogen from water splitting through either electrochemical process where electricity comes from renewable energy resources or photoelectrocatalytic route in which the semiconducting materials absorb sunlight and then generate an electron hole pair with the suitable potential to drive the hydrogen production [3–5]. One key step in water splitting is the hydrogen evolution reaction (HER, $2H^+ + 2e^- \rightarrow H_2$) and the catalysts play an important role in HER. Although noble platinum (Pt) metal exhibits excellent electrocatalytic activity and nearly no overpotential for HER, its high cost greatly restricts the massive production of hydrogen [6,7]. Therefore, exploring the low cost alternative to Pt catalyst has attracted considerable attention in the past few years. To date, a variety of materials including nickel

* Corresponding author. Tel.: +886 4 23590121.
E-mail address: twlin@thu.edu.tw (T.-W. Lin).

0926-3373/$ – see front matter © 2013 Elsevier B.V. All rights reserved.
http://dx.doi.org/10.1016/j.apcatb.2013.01.004

alloy [8–10], transition metal chalcogenides and carbides [11–15], and polymeric carbon nitride [16,17] have been tested to serve as the HER catalysts.

Molybdenum disulfide (MoS_2) is a semiconducting and layered material that exhibits versatile applications including lubricant, the catalyst for hydrodesulfuration, anode materials for lithium ion batteries and counter electrode in dye-sensitized solar cells [18–26]. Previous theoretical and experimental works have suggested that MoS_2 is a promising electrocatalyst for the HER and the HER activity is mainly derived from the edges of MoS_2 [27–29]. As a result, the number of exposed active sites in the edges is a crucial factor for the improvement of HER activity of MoS_2. Two strategies have been proposed to improve the catalytic activity of MoS_2 toward HER. One method involves the doping of MoS_2 with Co, which effectively decreases hydrogen binding energy of sulfur edges [30]. The other is to increase the amount of edges per mole MoS_2. Such method is well demonstrated by the recent study where MoS_2 nanoparticles are dispersed over the conductive graphene [31]. The high HER activity of the composite of MoS_2 nanoparticles and graphene can be attributed to the improvements in the amount of exposed edges per catalyst volume and the electrical contact between the MoS_2 nanoparticles and graphene. Furthermore, recent works have reported that amorphous molybdenum sulfide, MoS_3, can be synthesized at room temperature by either electrochemical method or wet chemistry process and the resulting MoS_3 thin films or nanoparticles exhibit high catalytic activity toward HER [32–34].

To the best of our knowledge, the nanocomposite of MoS_3 and multi-walled carbon nanotubes (MWCNTs) as HER catalyst has not been studied systematically. The participation of MWCNTs in the design of the catalyst should provide several advantages. First, due to their high surface area, MWCNTs enable the catalyst to be homogeneously dispersed over their surface. Second, the high conductivity of MWCNTs allows the electrons to be easily shuttled to the catalyst. Third, the great chemical and mechanical stability of MWCNTs should improve the stability of the catalyst in the long-term operation. Finally, MWCNTs are cheaper than other conductive carbon materials such as graphene. In this study, we report the synthesis of the nanocomposite of MoS_3 and MWCNTs (MoS_3/MWCNT-NC) using wet chemistry method. The composition, morphology and crystallinity of this nanocomposite are extensively characterized. To understand the origin of the HER activity of MoS_3/MWCNT-NC, the change in nanocomposite composition during catalysis and the effects of crystallinity and morphology on catalyst's activity are investigated. It is demonstrated that the MoS_3/MWCNT-NC exhibit excellent HER activity with a small overpotential (η) of ~0.13 V, large cathodic currents and a Tafel slope as small as 40 mV/decade. The high catalytic activity of MoS_3/MWCNT-NC is stemmed from the abundance of catalytic edge sites on MoS_3 nanoparticles and excellent electrical coupling to the conductive MWCNT network. Finally, it is demonstrated that MoS_3/MWCNT-NC possesses the reasonable stability in the long-term operation.

2. Experimental

2.1. Synthesis of MoS_3/MWCNT-NC

The functionalization of MWCNTs with carboxylic acid groups was achieved by refluxing MWCNTs (0.5 g) in conc. nitric acid (100 ml) at 120 °C for 12 h [35]. After the reaction, the MWCNT precipitate was filtered off, washed with distilled water and dried in air. For the synthesis of MoS_3/MWCNT-NC, acid-treated MWCNTs (20 mg) and ammonium tetrathiomolybdate (40, 80 and 160 mg) were mixed in 5 ml of 20% aqueous ethanol. The mixed solution was sonciated for 20 min to make a homogeneous dispersion and then 2 ml of concentrated HCl was added to the mixed solution. Upon the addition of HCl, the precipitation was observed due to the reaction: $(NH_4)_2MoS_4 + 2HCl \rightarrow MoS_3\downarrow + 2NH_4Cl + H_2S$. After a 2 h reaction time, the precipitate was filtered off, washed with distilled water and dried in air. In a control experiment, acid-treated MWCNTs were replaced by pristine MWCNTs and the aforementioned procedures were followed for the composite synthesis.

2.2. Material characterizations

Chemical compositions of the samples were determined by X-ray photoelectron spectroscope (XPS, Phi V5000). XPS measurements were performed with an Al Kα X-ray source. The energy calibrations were made against the C 1s peak to eliminate the charging of the sample during analysis. X-ray powder diffraction (XRD) pattern of the nanocomposite was obtained from Philips X'Pert Pro MPD. Field-emission transmission electron microscope (TEM, JEOL JEM-2100F, operated at 200 kV with a point-to-point resolution of 0.19 nm) equipped with an energy dispersive spectrometer (EDS) was used to obtain the information on the microstructures and the chemical compositions.

2.3. Electrochemical characterizations

In the study of the HER activity of the nanocomposite, 1 mg of catalyst and 80 μl of 5 wt% Nafion solution were mixed in 10 ml of ethanol and the mixed solution was sonicated for 10 min to form a homogeneous ink. Then the catalyst ink was drop-cast onto a silver electrode of 5 mm in diameter, which serves as the working electrode. Linear sweep voltammetry (Autolab PGSTAT-128N) with scan rate of 1 mV s^{-1} was conducted in a 1 M H_2SO_4 solution using Ag/AgCl as the reference electrode and a Pt as the counter electrode The electrochemical impedance spectroscopy (EIS) measurements were performed in the same configuration at $\eta = 0.17$ V from 10^6 to 0.02 Hz with an AC voltage of 5 mV. The complex nonlinear least square (CNLS) analyses of the resulting EIS spectra were conducted using the software ZSimpWin version 3.1. The standard error after the best-fit values for each equivalent circuit parameter is less than 5% when using the proposed equivalent circuit model in this study.

3. Results and discussion

3.1. Structural and compositional characterization of MoS_3/MWCNT-NC

Fig. 1a is the TEM image of acid-treated MWCNTs showing that a few of amorphous carbon impurities are deposited on MWCNT surface. Comparatively, Fig. 1b–d shows the typical TEM images of the MWCNTs loaded with the various amount of MoS_3. The weight percentage of MoS_3 loaded on MWCNTs is increased with the concentration of ammonium tetrathiomolybdate and ranges from 9% to 69%. For the MWCNT composite with 33 wt% MoS_3 (MoS_3(33%)/MWCNT-NC), the corresponding TEM image (Fig. 1b) shows some nanoparticles are dispersed over the MWCNT surface. In Fig. 1c, it is noted for the MWCNT composite with 50 wt% MoS_3 (MoS_3(50%)/MWCNT-NC) that the MoS_3 nanoparticles are aggregated to form the partial coating on the MWCNT surface. As shown in Fig. 1d, MWCNT surface is fully covered with a thick amorphous layer when the loading amount of MoS_3 on MWCNTs is 69 wt% (MoS_3(69%)/MWCNT-NC). The EDS analysis of the composite samples (see Fig. S1) reveals the presence of C, O, Mo and S elements. To further characterize the identity and structure of the composite sample, XRD measurement was carried out. As shown in Fig. S2, the peaks at 25.8° and 44.6° are indexed to (0 0 2) and (1 0 0) reflections of MWCNTs, respectively [36]. Based on the fact that only MWCNT diffraction peaks are observed in the spectrum, it is confirmed that

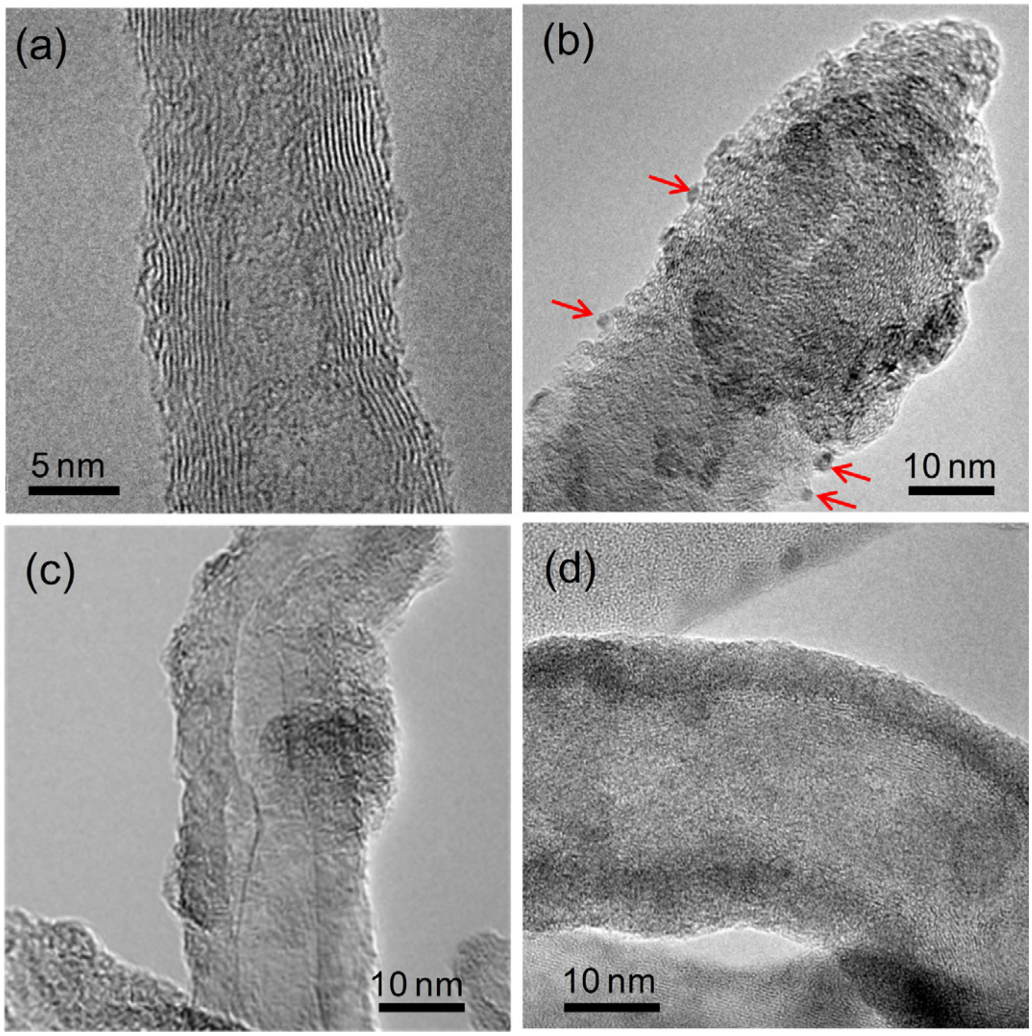

Fig. 1. Typical TEM images of (a) acid-treated MWCNTs, (b) MoS_3(33%)/MWCNT-NC, (c) MoS_3(50%)/MWCNT-NC and (d) MoS_3(69%)/MWCNT-NC. The red arrows in (b) indicate the presence of MoS_3 nanoparticles on MWCNT surface. (For interpretation of the references to color in this figure legend, the reader is referred to the web version of this article.)

MoS_3 is noncrystalline, which is consistent with the previous report [37].

Fig. 2 shows the XPS spectra of the MoS_3/MWCNT-NC. The C 1s core level shown in Fig. 2b can be deconvoluted into five peaks. The main peak at 284.6 eV is assigned to sp^2-hybridized graphite-like carbon atoms. The peak at 285.3 eV is attributed to sp^3-hybridized carbon atoms whereas the peaks at 286.2, 287.2 and 288.9 eV are the carbon atoms bound to one oxygen atom by a single bond, by a double bond and to two oxygen atoms, respectively. These binding energies are all consistent with the reported values for acid-treated MWCNTs [38]. As shown in Fig. 2c, the Mo3d signal consists of two doublets. The doublet (Mo $3d_{5/2}$ = 229.6 eV; Mo $3d_{3/2}$ = 232.9 eV) at a relatively lower binding energy can be assigned to the Mo ion in +4 oxidation state whereas the other doublet (Mo $3d_{5/2}$ = 232.6 eV; Mo $3d_{3/2}$ = 235.8 eV) is attributed to Mo ion in MoO_3 which may be formed during the preparation of the catalyst [39]. Fig. 2d shows that the S 2p peak can also be deconvoluted into two doublets. The doublet at a relatively higher binding energy (S $2p_{3/2}$ = 163.5 eV; S $2p_{1/2}$ = 164.5 eV) is assigned to bridging ${S_2}^{2-}$ and/or apical S^{2-} ligands whereas the other (S $2p_{3/2}$ = 162.3 eV; S $2p_{1/2}$ = 163.5 eV) is attributed to the terminal ${S_2}^{2-}$ and/or S^{2-} [40,41]. Two doublets show an intensity ratio of 5:4, favoring the doublet with a higher binding energy. Based on the peak area of each elemental spectrum, the atomic ratio of Mo(IV) to S is estimated to be 1:3.1. Therefore, the composition of the amorphous coating on the MWCNT surface is assigned to MoS_3.

3.2. Electrocatalytic activity of MoS_3/MWCNT-NC toward HER

To test the catalytic activity of the MoS_3/MWCNT-NC toward HER, MoS_3(69%)/MWCNT-NC was drop-cast onto the Ag electrode and then the polarization measurement was carried out in a 1 M H_2SO_4 solution. The catalytic activity of the silver electrode was firstly examined, which shows no HER activity (Fig. S3). Fig. 3a shows the first polarization curve of MoS_3(69%)/MWCNT-NC, which displays a highly catalytic activity toward HER. It is noteworthy that there is a broad reduction peak at potential more positive than the HER potential and this reduction peak is absent in the subsequent scans. The presence of reduction peak suggests that MoS_3 acts as the precatalyst. To find out the actual catalyst for HER, MoS_3(69%)/MWCNT-NC after five polarization scans was analyzed by XPS. As shown in Fig. S4, the shape of S spectrum of the nanocomposite after five scans shows an obvious change and the location of main peak shifts to the lower binding energy compared with that in MoS_3 (Fig. 2d). Furthermore, the S 2p peak can be deconvoluted into two doublets. The doublet at a relatively higher binding energy (S $2p_{3/2}$ = 162.5 eV; S $2p_{1/2}$ = 163.7 eV) is consistent with the reported values for MoS_2 [40]. The other (S $2p_{3/2}$ = 161.5 eV;

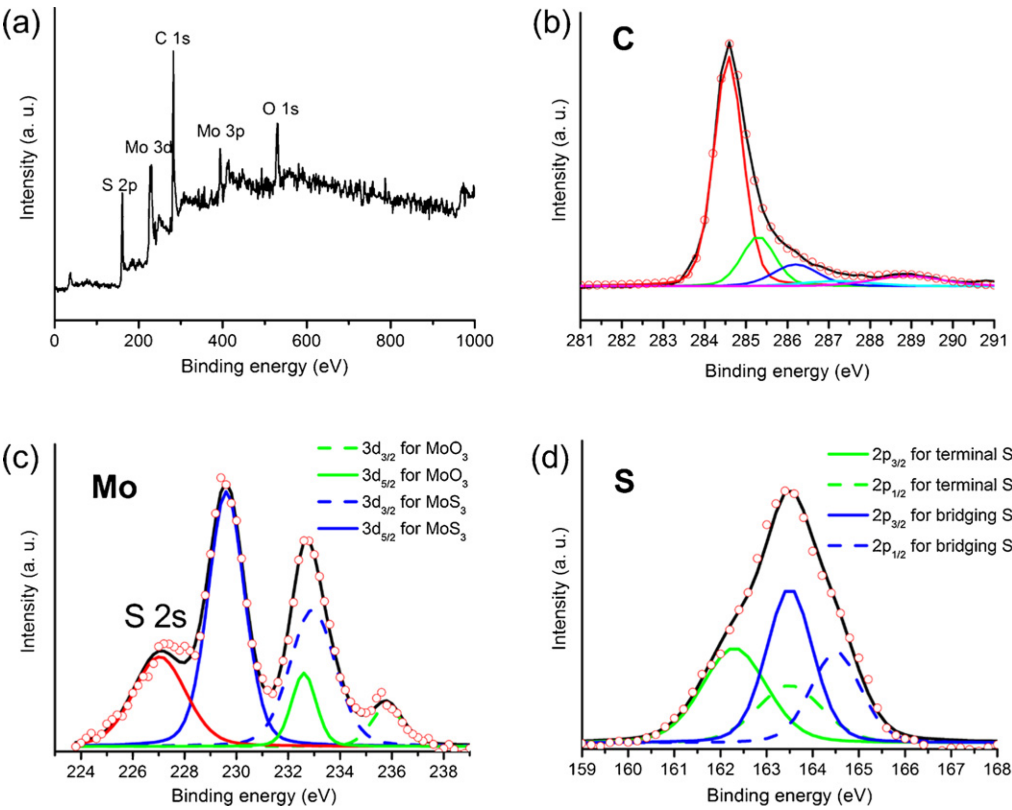

Fig. 2. (a) XPS survey spectra and (b–d) high-resolution XPS analysis of the MoS_3/MWCNT-NC.

S $2p_{1/2}$ = 162.7 eV) can be attributed to the contribution from Ag_2S which is possibly formed in the reaction between the released S^{2-} and Ag electrode [42]. Based on the peak area of each elemental spectrum, the atomic ratio of Mo(IV) to S (the doublet at 162.5 eV and 163.7 eV) is estimated to be 1:2.1. Therefore, it is concluded that the amorphous MoS_3 on the MWCNTs is reduced to MoS_2 during the first polarization and the amorphous MoS_2 is then served as the actual catalyst for HER. This result is consistent with the previous study where Merki et al. report an electrochemical reduction of MoS_3 to form MoS_2 as the active specie for HER [32].

Since the MoS_2 is identified as the actual catalyst for HER, the effect of MoS_2 crystallinity on catalytic activity is investigated. For the MoS_3(69%)/MWCNT-NC annealed at 350 °C in H_2 for 1 h, XRD measurement shows that it still has the amorphous structure (Fig. S5). As the annealing temperature is elevated, MoS_3 is reduced to MoS_2 and the crystallinity of MoS_2 is gradually improved based on the value of the full width at half maximum (FWHM) of the (1 0 0) reflection of MoS_2. Fig. 3b–d shows the polarization curves of the MoS_3(69%)/MWCNT-NC annealed at various temperatures. It is noted that reduction peak is absent in these first polarization curves. Furthermore, the current densities of the nanocomposites significantly decrease with increasing annealing temperatures, suggesting a gradual loss of catalytic activity. The previous studies show that the HER activity of MoS_2 is correlated to the amount of exposed edges and the improved crystallinity of the MoS_2 catalyst leads to reduction of the edge amount and thus loss of HER activity [28,34]. The similar trend is also observed in the current study. Compared with the annealed MWCNT nanocomposites, MoS_3/MWCNT-NC exhibits the higher HER activity due to the fact that its amorphous structure imparts a higher number of exposed edges [34]. Therefore, the following discussions are mainly focused on MoS_3/MWCNT-NC.

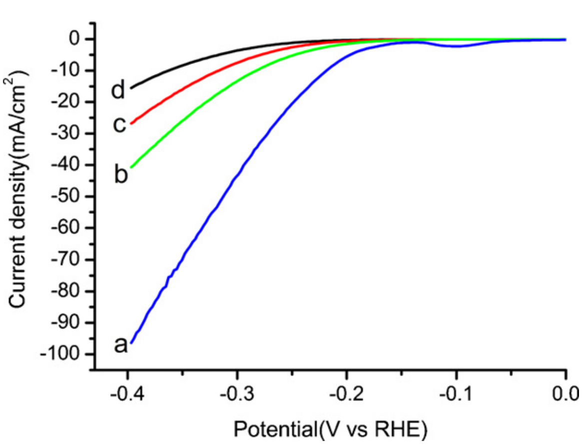

Fig. 3. Polarization curves of (a) MoS_3(69%)/MWCNT-NC, (b) MoS_3(69%)/MWCNT-NC after annealing at 350 °C, (c) MoS_3(69%)/MWCNT-NC after annealing at 450 °C, and (d) MoS_3(69%)/MWCNT-NC after annealing at 650 °C. In each measurement, the composite of 510 μg/cm^2 was deposited onto silver electrode.

The effect of the loading amount of MoS_3 on MWCNT surface on HER activity is investigated. Fig. 4 shows the polarization curves of the MWCNT composites loaded with the various amount of MoS_3(9–69 wt%). The dependence of HER activity on the loading amount of MoS_3 is observed. The catalytic activity of MoS_3/MWCNT-NC is increased with decreasing the MoS_3 loading on MWCNTs. When the MoS_3 loading is 69 wt%, the relatively low catalytic activity is observed. Comparatively, the optimal MoS_3 loading on MWCNTs is 33 wt%, which shows the highest catalytic activity among all the composite catalysts. Under this condition, the current densities are 1.120 and 10.83 mA cm^{-2} at η = 150 and 200 mV, respectively. However, if the MoS_3 loading on the MWCNT surface is too low (9 wt%), there is no sufficient catalyst for HER

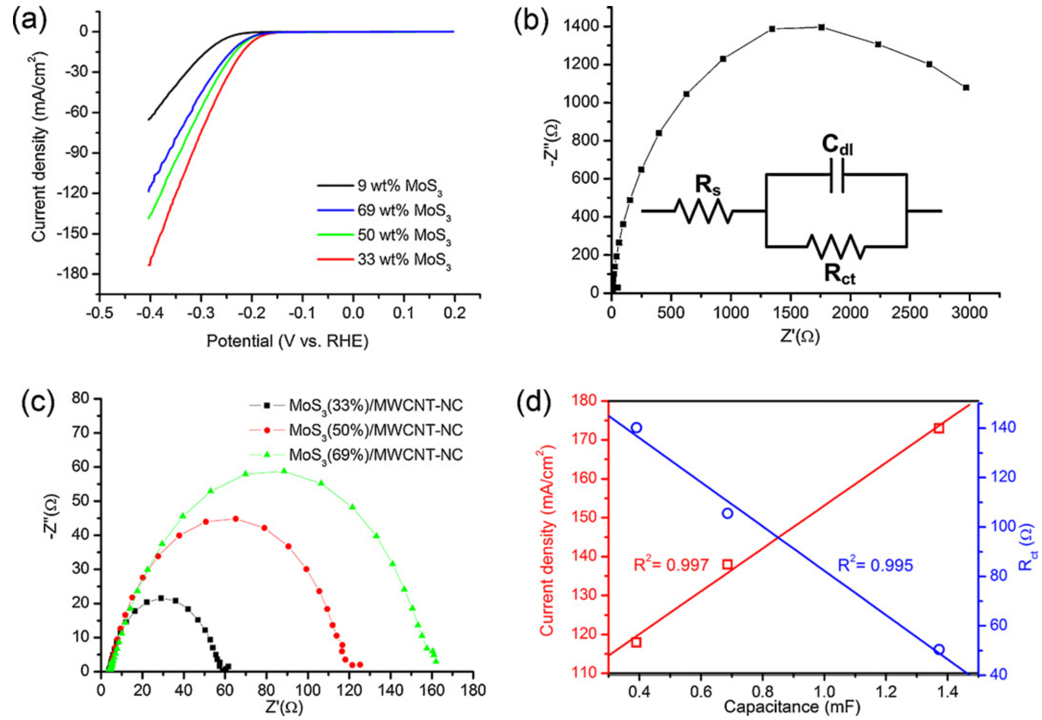

Fig. 4. (a) Polarization curves of MWCNT composites loaded with various amount of MoS_3. In each measurement, the composite of 255 μg/cm² was deposited onto silver electrode. (b) Nyquist plot of MoS_3(9%)/MWCNT-NC. The inset shows the equivalent circuit used for fitting the EIS results. (c) Nyquist plots of MoS_3(33%)/MWCNT-NC, MoS_3(50%)/MWCNT-NC and MoS_3(69%)/MWCNT-NC. (d) HER activity of MWCNT composites loaded with various amount of MoS_3 as a function of the C_{dl}. The current density of the catalyst was measured from a at $\eta = 0.4$ V.

and thus the relatively low catalytic activity is observed. The difference in catalytic activity among the various nanocomposites may be correlated to the active surface area of MoS_3 which is dependent on the MoS_3 morphology on the MWCNT surface. For the MoS_3(69%)/MWCNT-NC, the thick MoS_3 layers formed on MWCNT walls are observed (Fig. 1d). Comparatively, TEM image of MoS_3(33%)/MWCNT-NC (Fig. 1b) shows that many small MoS_3 nanoparticles are dispersed over the MWCNT surface. These MoS_3 nanoparticles presumably have the large contact area with the electrolyte and thus exhibit the high catalytic activity.

To further investigate the effect of active surface area of the catalyst on the HER activity, we preformed the EIS analysis of the MWCNT composites loaded with various amount of MoS_3(9–69%). For the MoS_3(9%)/MWCNT-NC, the obtained Nyquist plot is shown in Fig. 4b. The intercept of the semicircle on the real axis is assigned to the ohmic series resistance (R_s). The semicircle in the high-frequency range of the Nyquist plot is attributed to the resistance capacitance (RC) network, consisting of the charge transfer resistance (R_{ct}) of H^+ reduction and the corresponding capacitance (C_{dl}) at the electrode–electrolyte interface [43,44]. Table 1 summarizes the values of R_{ct} and C_{dl} estimated by fitting the arc observed at high frequency with Zsimpwin software in terms of the equivalent circuit model (the inset in Fig. 4b). It is noted that the R_{ct} value of MoS_3(9%)/MWCNT-NC is the largest among all the composite catalysts; therefore, MoS_3(9%)/MWCNT-NC shows the worst HER activity, which is consistent with the result obtained from polarization measurements (Fig. 4a). In contrast, MoS_3(33%)/MWCNT-NC has the low R_{ct} value of 50.4 Ω and thus shows superior HER activity to other composite catalysts as shown in Fig. 4c. It is noted from Table 1 that MoS_3(33%)/MWCNT-NC has the largest C_{dl} value among all the composite catalysts. The large C_{dl} value of the MoS_3(33%)/MWCNT-NC corresponds to its large active surface area, which can highly promote the HER activity of the MoS_3(33%)/MWCNT-NC [43,44]. Fig. 4d shows the correlation of active surface area of the composite catalysts to their HER activity. Without the inclusion of MoS_3(9%)/MWCNT-NC, it is found that the current density (R_{ct} value) of the catalyst linearly increases (decreases) with the C_{dl} value, which indicates that the active surface area of the catalyst contributes greatly to HER activity. For example, MoS_3(33%)/MWCNT-NC has the highest C_{dl} value (or the largest active surface); therefore, its HER activity is the highest among all the composite catalysts. The observed dependence of HER activity of the catalyst on the active surface area is in accordance with the previous study reported by Benck et al. [33].

The effect of the loading amount of MoS_3(33%)/MWCNT-NC on the electrode on the catalytic activity is also examined. As shown in Fig. 5, the current density increases with the loading amount of composite catalyst on the electrode but gradually approaches the saturation at high loading amount (Fig. S6). The onset overpotential for HER ranges from 130 mV to 150 mV. Table 2 summarizes the HER activities of the electrodes loaded with various amount of MoS_3(33%)/MWCNT-NC based on polarization measurements. When the electrode is loaded with the nanocomposite of 255 μg/cm², the Tafel slope of 40 mV/decade is observed (the inset in Fig. 5). This value is comparable to that of MoS_2 nanoparticles deposited on reduced graphene oxide [31]. As remarked by Li et al. [31], such small Tafel slope suggests

Table 1
EIS parameters of MWCNT composites loaded with various amount of MoS_3.

	C_{dl} (mF)	R_{ct} (Ω)	Current density (mA/cm²)[a]
MoS_3(9%)/MWCNT-NC	0.54	2808	65
MoS_3(33%)/MWCNT-NC	1.37	50.4	173
MoS_3(50%)/MWCNT-NC	0.69	105.6	138
MoS_3(69%)/MWCNT-NC	0.39	140.3	118

[a] Each current density was measured at $\eta = 0.4$ V.

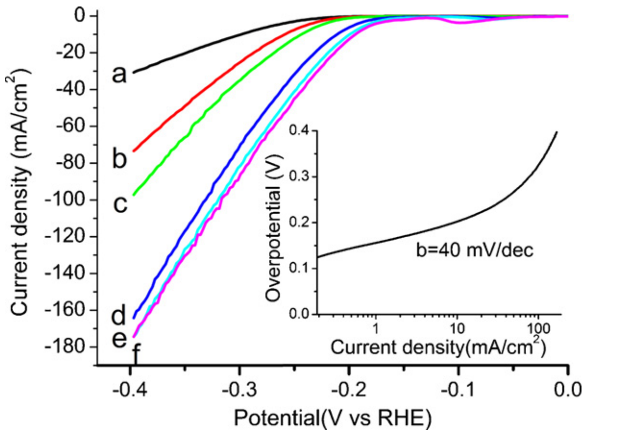

Fig. 5. Polarization curves of the silver electrodes loaded with MoS_3(33%)/MWCNT-NC of (a) 5.1 μg/cm^2, (b) 25.5 μg/cm^2, (c) 51 μg/cm^2, (d) 153 μg/cm^2, (e) 255 μg/cm^2 (cyan line) and (f) 510 μg/cm^2 (purple line). The inset shows Tafel plot for the silver electrode loaded with MoS_3(33%)/MWCNT-NC composite of 255 μg/cm^2.

that electrochemical desorption is the rate-limiting step and thus the Volmer–Heyrovsky mechanism is responsible for the HER catalyzed by the MoS_3/MWCNT-NC.

Several control experiments are performed to verify that the high HER activity of MoS_3/MWCNT-NC is derived from strong chemical and electronic coupling between the MWCNTs and MoS_3. Fig. 6a shows that free MWCNTs or MoS_3 powder alone exhibit little HER activity. Furthermore, 33 wt% MoS_3 particles physically mixed with MWCNTs shows the inferior HER activity to MoS_3(33%)/MWCNT-NC. This result suggests that the electron transfer from MWCNTs to MoS_3 precatalyst is significantly improved when MoS_3 is directly deposited onto MWCNT surface. It is also noted that the use of acid-treated MWCNTs affects the catalytic performance of the nanocomposite toward HER. As shown in Fig. 6a, although pristine MWCNTs have a similar loading amount of MoS_3 to acid-treated MWCNTs, the former exhibits the lower HER activity than the later. As shown in Fig. 6b, TEM analysis of pristine MWCNTs loaded with 40 wt% MoS_3 shows that MoS_3 is aggregated to form a layer of coating on MWCNT surface. In sharp contrast, MoS_3 nanoparticles are formed on acid-treated MWCNT surface (Fig. 1b), which indicates that the presence of functional groups in MWCNTs may allow the growth of highly dispersed MoS_3 nanoparticles on MWCNTs. The small size and high dispersion of MoS_3 nanoparticles on MWCNTs should afford the large contact surface between MoS_3 and the electrolyte, which leads to the improved HER activity. As shown in Fig. S7, MoS_3(33%)/MWCNT-NC has the smallest value of Tafel slope (45 mV/decade) and exhibits the best catalytic performance toward HER among all the catalysts. The high HER activity of MoS_3(33%)/MWCNT-NC is attributed to the synergistic effect from the conductive network of MWCNTs and the large active surface area of MoS_3 nanoparticles. To further verify this effect, the impedance measurements on MoS_3(33%)/MWCNT-NC and MoS_3 powder were performed. As shown in Fig. 6c, the R_{ct} value (1349 Ω) of MoS_3(33%)/MWCNT-NC is considerably lower than that of MoS_3 powder (R_{ct} = 9577 Ω), suggesting that MoS_3(33%)/MWCNT-NC has rapider electron-transfer kinetics at the electrode/electrolyte interface. The high HER activity of MoS_3(33%)/MWCNT-NC is attributed to the fact that the composite catalyst possesses the larger active surface area than MoS_3 powder. It is noteworthy that the C_{dl} value of MoS_3(33%)/MWCNT-NC is 0.1 mF, which is about ten times larger than that of MoS_3 powder (0.013 mF). In addition, the R_s value of the MoS_3(33%)/MWCNT-NC (4.69 Ω) is lower than that of the MoS_3 powder (5.20 Ω) due to the superior electrical conductivity of MWCNTs. Finally, the test of long-term stability of MoS_3(33%)/MWCNT-NC was performed. As shown in Fig. 6d, the current density gradually decreases from its initial value to 88% after the continuous 500 cycling.

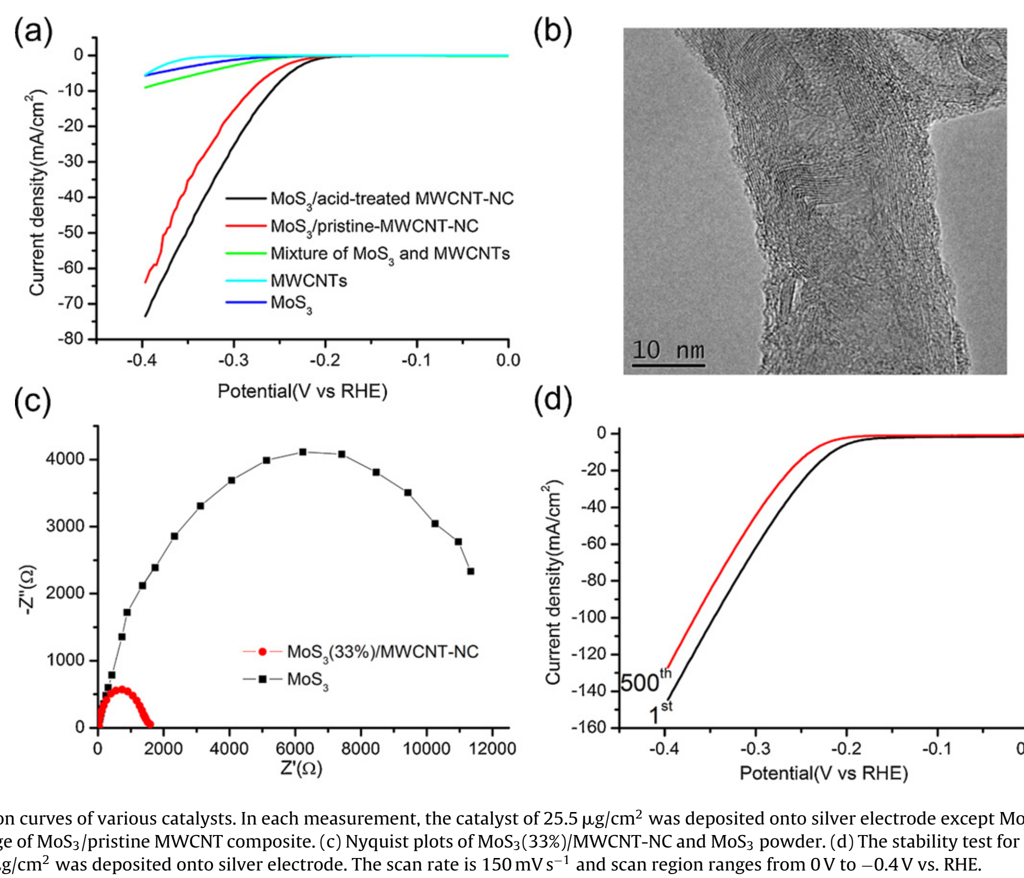

Fig. 6. (a) Polarization curves of various catalysts. In each measurement, the catalyst of 25.5 μg/cm^2 was deposited onto silver electrode except MoS_3 powder (8.4 μg/cm^2). (b) Typical TEM image of MoS_3/pristine MWCNT composite. (c) Nyquist plots of MoS_3(33%)/MWCNT-NC and MoS_3 powder. (d) The stability test for MoS_3(33%)/MWCNT-NC. The catalyst of 255 μg/cm^2 was deposited onto silver electrode. The scan rate is 150 mV s^{-1} and scan region ranges from 0 V to −0.4 V vs. RHE.

Table 2
HER activity of the silver electrodes loaded with various amount of MoS_3(33%)/MWCNT-NC.

Loading (μg/cm^2)	Tafel slope (mV/decade)	Exchange current density (A/cm^2)	$j_{\eta=150}$ (mA cm^{-2})	$j_{\eta=200}$ (mA cm^{-2})
5.1	57[a]	1.43×10^{-7}	0.052	0.349
25.5	45[b]	3.38×10^{-8}	0.095	0.676
51	41[c]	2.88×10^{-8}	0.159	1.292
153	39[d]	5.37×10^{-8}	0.632	6.634
255	40[e]	1.35×10^{-7}	1.120	10.83
510	42[f]	3.52×10^{-7}	2.048	13.32

[a] Determined at η = 208–240 mV.
[b] Determined at η = 181–220 mV.
[c] Determined at η = 167–206 mV.
[d] Determined at η = 147–186 mV.
[e] Determined at η = 135–174 mV.
[f] Determined at η = 126–165 mV.

The loss in activity may be stemmed from catalyst poisoning or the detachment of the catalyst from the substrate [33]. Overall, MoS_3/MWCNT-NC shows an excellent HER activity and the reasonable stability in the long-term operation.

According to the Tafel equation ($j = -j_0 e(-\eta/b)$, where j is the current density, J_0 is the exchange current density and b is the Tafel slope), the optimal catalyst should have a low Tafel slope and a large exchange current density to produce the highest currents at the least overpotential [28]. Herein, it is attempted to make the comparison of HER activity between MoS_3/MWCNT-NC and MoS_x (x = 2 or 3) based catalysts. As a reference point, we performed polarization measurements on the sputtered Pt electrode. As shown in Fig. S8, the sputtered Pt electrode has a near zero overpotential and exhibits high HER activity ($j_{\eta=150}$ = 95 mA/cm^2; b = 37 mV/decade; $J_0 = 1.1 \times 10^{-4}$ A/cm^2). There are some reports associated with HER activities of MoS_3 thin films and nanoparticles prepared by wet chemistry method [33,34]. The Tafel slopes observed for the MoS_3 thin film (60 mV/decade) and MoS_3 nanoparticles (40–63 mV/decade) are higher than those of MoS_3(33%)/MWCNT-NC (39–57 mV/decade) [33,34]. Furthermore, the Tafel slopes observed in the current study are even much lower than those of MoS_2 nanotriangles (55–60 mV/decade) [45], MoS_2 nanoparticles (120 mV/decade) [30], and MoS_2/graphene nanocomposites (58–92 mV/decade) reported by Firmiano et al. [46]. In addition to Tafel slope, the exchange current density is another inherent measure of HER activity of the catalyst. The exchange current densities of MoS_3(33%)/MWCNT-NC range from 2.9×10^{-8} A/cm^2 to 3.5×10^{-7} A/cm^2, which are comparable to those of MoS_2 nanotriangles ($1.3–3.1 \times 10^{-7}$ A/cm^2) [45], MoS_3 thin film (1.3×10^{-7} A/cm^2) and MoS_3 nanoparticles ($2 \times 10^{-8}–1 \times 10^{-6}$ A/cm^2) [32,34]. Compared with the aforementioned MoS_x catalysts, the advantages of MoS_3/MWCNT-NC include higher HER activity, easier preparation and lower production cost.

4. Conclusions

The nanocomposite of MoS_3 and MWCNTs with the high catalytic activity toward HER can be easily synthesized by wet chemistry process. It is found that the functional groups in acid-treated MWCNTs allow the growth of highly dispersed MoS_3 nanoparticles on the MWCNT surface. According to XPS data, amorphous MoS_3 on the MWCNTs is reduced to MoS_2 during the first polarization and thus the amorphous MoS_2 is identified as the actual catalyst for HER. It is noted that MoS_2 with amorphous structure exhibits the higher HER activity than crystalline MoS_2 due to the fact that the former has a higher number of exposed edges. Furthermore, it is observed that the catalytic activity of MoS_3/MWCNT-NC is increased with decreasing the MoS_3 loading on MWCNTs and the optimal loading amount of MoS_3 on MWCNTs is 33 wt%. Based on the extensive TEM analysis and capacitance measurements, the catalytic activity of the nanocomposites is correlated to the active surface area of MoS_3 which is dominated by MoS_3 morphology on the MWCNT surface. The MoS_3(33%)/MWCNT-NC exhibits excellent HER activity with a small overpotential of ~0.13 V, large cathodic currents and a Tafel slope as small as 40 mV/decade. The high catalytic activity of MoS_3(33%)/MWCNT-NC is stemmed from a high number of exposed edges of amorphous MoS_3 nanoparticles and excellent electrical coupling to the conductive MWCNT network as evidenced by the impedance measurements. Furthermore, it is found that the current density of MoS_3(33%)/MWCNT-NC is decreased to 88% of the initial value after the continuous 500 cycling, which shows the reasonable stability in the long-term operation. The present work suggests that the highly active and stable MoS_3(33%)/MWCNT-NC shows a great potential as a low cost alternative to Pt in water splitting.

Acknowledgements

This research was supported by National Science Council Taiwan (NSC 101-2113-M-029-003). This research was also supported by the program of Global Research & Education on Environment and Society (GREEnS) of Tunghai University. We also thank Dr. Yi-Hsien Lee for his assistance with the XPS measurements.

Appendix A. Supplementary data

Supplementary data associated with this article can be found, in the online version, at http://dx.doi.org/10.1016/j.apcatb.2013.01.004.

References

[1] J.A. Turner, Science 305 (2004) 972.
[2] J. Nowotny, C.C. Sorrell, L.R. Sheppard, T. Bak, International Journal of Hydrogen Energy 30 (2005) 521.
[3] P.D. Tran, L.H. Wong, J. Barber, J.S.C. Loo, Energy & Environmental Science 5 (2012) 5902.
[4] X.J. Lv, W.F. Fu, H.X. Chang, H. Zhang, J.S. Cheng, G.J. Zhang, Y. Song, C.Y. Hu, J.H. Li, Journal of Materials Chemistry 22 (2012) 1539.
[5] M.G. Walter, E.L. Warren, J.R. McKone, S.W. Boettcher, Q.X. Mi, E.A. Santori, N.S. Lewis, Chemical Reviews 110 (2010) 6446.
[6] L.A. Kibler, ChemPhysChem 7 (2006) 985.
[7] R. Subbaraman, D. Tripkovic, D. Strmcnik, K.C. Chang, M. Uchimura, A.P. Paulikas, V. Stamenkovic, N.M. Markovic, Science 334 (2011) 1256.
[8] N.V. Krstajic, V.D. Jovic, L. Gajic-Krstajic, B.M. Jovic, A.L. Antozzi, G.N. Martelli, International Journal of Hydrogen Energy 33 (2008) 3676.
[9] A. Lasia, A.J. Rami, Journal of Electroanalytical Chemistry 294 (1990) 123.
[10] S.A.S. Machado, L.A. Avaca, Electrochimica Acta 39 (1994) 1385.
[11] M.R. Gao, Z.Y. Lin, T.T. Zhuang, J. Jiang, Y.F. Xu, Y.R. Zheng, S.H. Yu, Journal of Materials Chemistry 22 (2012) 13662.
[12] A. Sobczynsk, A. Yildiz, A.J. Bard, A. Campion, M.A. Fox, T. Mallouk, S.E. Webber, J.M. White, Journal of Physical Chemistry 92 (1988) 2311.
[13] Z. Wu, B. Fang, A. Bonakdarpour, A. Sun, D.P. Wilkinson, D. Wang, Applied Catalysis B: Environmental 125 (2012) 59.

[14] F. Harnisch, G. Sievers, U. Schröder, Applied Catalysis B: Environmental 89 (2009) 455.
[15] S. Wirth, F. Harnisch, M. Weinmann, U. Schröder, Applied Catalysis B: Environmental 126 (2012) 225.
[16] X. Wang, K. Maeda, X. Chen, K. Takanabe, K. Domen, Y. Hou, X. Fu, M. Antonietti, Journal of the American Chemical Society 131 (2009) 1680.
[17] J. Zhang, M. Zhang, G. Zhang, X. Wang, ACS Catalysis 2 (2012) 940.
[18] E. Benavente, M.A. Santa Ana, F. Mendizabal, G. Gonzalez, Coordination Chemistry Reviews 224 (2002) 87.
[19] X. Zhou, L.J. Wan, Y.G. Guo, Nanoscale 4 (2012) 5868.
[20] M.X. Wu, Y. Wang, X. Lin, N. Yu, L. Wang, A. Hagfeldt, T.L. Ma, Physical Chemistry Chemical Physics 13 (2011) 19298.
[21] J. Xiao, D. Choi, L. Cosimbescu, P. Koech, J. Liu, J.P. Lemmon, Chemistry of Materials 22 (2010) 4522.
[22] K. Chang, W. Chen, Chemical Communications 47 (2011) 4252.
[23] Kun Chang, W. Chen, L. Ma, H. Li, H. Li, F. Huang, Z. Xu, Q. Zhang, J.Y. Lee, Journal of Materials Chemistry 21 (2011) 6251.
[24] F.Y. Cheng, J. Chen, X.L. Gou, Advanced Materials 18 (2006) 2561.
[25] J.J. Lee, H. Kim, S.H. Moon, Applied Catalysis B: Environmental 41 (2003) 171.
[26] C.J. Liu, S.Y. Tai, S.W. Chou, Y.C. Yu, K.D. Chang, S. Wang, F.S.S. Chien, J.Y. Lin, T.W. Lin, Journal of Materials Chemistry 22 (2012) 21057.
[27] D. Merki, X. Hu, Energy & Environmental Science 4 (2011) 3878.
[28] A.B. Laursen, S. Kegnæs, S. Dahl, I. Chorkendorff, Energy & Environmental Science 5 (2012) 5577.
[29] Z. Chen, D. Cummins, B.N. Reinecke, E. Clark, M.K. Sunkara, T.F. Jaramillo, Nano Letters 11 (2011) 4168.
[30] J. Bonde, P.G. Moses, T.F. Jaramillo, J.K. Nørskov, I. Chorkendorff, Faraday Discussions 140 (2009) 219.
[31] Y. Li, H. Wang, L. Xie, Y. Liang, G. Hong, H. Dai, Journal of the American Chemical Society 133 (2011) 7296.
[32] D. Merki, S. Fierro, H. Vrubel, X. Hu, Chemical Science 2 (2011) 1262.
[33] J.D. Benck, Z. Chen, L.Y. Kuritzky, A.J. Forman, T.F. Jaramillo, ACS Catalysis 2 (2012) 1916.
[34] H. Vrubel, D. Merki, X. Hu, Energy & Environmental Science 5 (2012) 6136.
[35] T.W. Lin, C.G. Salzmann, L. Shao, C.H. Yu, M.L.H. Green, S.C. Tsang, Carbon 47 (2009) 1415.
[36] C. Pirlot, I. Willems, A. Fonseca, J.B. Nagy, J. Delhalle, Advanced Engineering Materials 4 (2002) 109.
[37] Y.V. Shubin, L.G. Bulusheva, Inorganic Materials 43 (2007) 236.
[38] T.I.T. Okpalugo, P. Papakonstantinou, H. Murphy, J. McLaughlin, N.M.D. Brown, Carbon 43 (2005) 153.
[39] T. Weber, J.C. Muijsers, J.H.M.C. van Wolput, C.P.J. Verhagen, J.W. Niemantsverdriet, Journal of Physical Chemistry 100 (1996) 14144.
[40] J. Iranmahboob, S.D. Gardner, H. Toghiani, D.O. Hill, Journal of Colloid and Interface Science 270 (2004) 123.
[41] T. Weber, J.C. Muijsers, J.W. Niemantsverdriet, Journal of Physical Chemistry 99 (1995) 9194.
[42] C. Zou, M. Li, L. Zhang, Y. Yang, Q. Li, X. Chen, X. Xu, S. Huang, CrystEngComm 13 (2011) 3515.
[43] J. Kubisztal, A. Budniok, A. Lasia, International Journal of Hydrogen Energy 32 (2007) 1211.
[44] I. Dannee, S. Noori, International Journal of Hydrogen Energy 36 (2011) 12102.
[45] T.F. Jaramillo, K.P. Jørgensen, J. Bonde, J.H. Nielsen, S. Horch, I. Chorkendorff, Science 317 (2007) 100.
[46] E.G.S. Firmiano, M.A.L. Cordeiro, A.C. Rabelo, C.J. Dalmaschio, A.N. Pinheiro, E.C. Pereira, E.R. Leite, Chemical Communications 48 (2012) 7687.